AJP

ISSN : 0971 - 3093

Vol 34, Nos 3 & 4, March-April, 2025

ASIAN JOURNAL OF PHYSICS

An International Peer Reviewed Research Journal

P K Kaw Memorial Issue

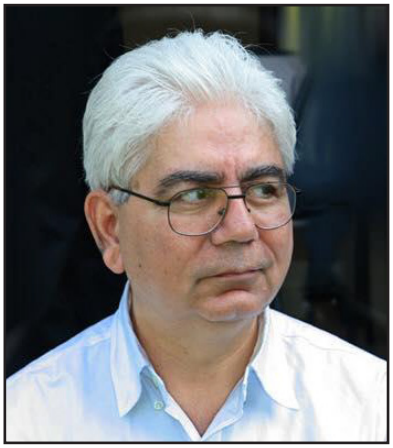

Prof P K Kaw

Guest Editors : Ramesh Narayanan & Satyananda Kar

ap

ANITA PUBLICATIONS

FF-43, 1st Floor, Mangal Bazar, Laxmi Nagar, Delhi-110 092, India

B O : 2, Pasha Court, Williamsville, New York-14221-1776, USA

Asian Journal of Physics
Vol. 34, Nos 3 & 4 (2025) 223-235
Available on: www.asianjournalofphysics.com

ap

The effect of rotating transverse magnetic field on plasma parameters in capacitively coupled discharges

Anuravi Sharma, and R Narayanan

Department of Energy Science and Engineering,

Indian Institute of Technology Delhi, Hauz Khas, New Delhi-110 016, India

Dedicated to Prof P K Kaw

This paper presents the results of placing a set of permanent ring magnets in a direction perpendicular to the parallel plate electrodes of the rf plasma discharge chamber. The influence of static transverse magnetic field, i.e. parallel to the surface of electrodes on plasma parameters has been discussed. Based on the application under study, the process would require a desired ion flux with a directed and adjustable ion energy bombarding the substrate. For controlling these two parameters, one needs to control the plasma density and DC bias across the sheath which directly depends on the plasma profiles and power coupling mechanisms. The present work is mainly devoted to experimentally verifying the variation of plasma parameters as a function of discharge pressure and spatial variation to provide qualitative perception in understanding the role of transverse magnetic field in capacitive discharges.

doi: 10.54955/AJP.34.3-4.2025.223-235

Keywords: Rotating transverse magnetic field, $\vec{E}\times\vec{B}$ drift, Ring magnets, Electron gyrofrequency.

1 Introduction

Capacitively Coupled Discharges (CCDs), operated usually at fundamental radio frequency (13.56 MHz) or higher frequencies in the range (27.12-160) MHz are the commonly used plasma devices for industrial processes namely etching, sputtering, surface treatment, material processing etc. [1-4]. Ion flux and ion energy bombarding the target material are two principal parameters that decide the optimization and output of industrial processes. Magnetized Capacitive Discharges, i.e. discharges with externally applied magnetic field are used as an alternative scheme to overcome the constraint of independent control of ion flux and ion energy that cannot be made possible with conventional single frequency CCDs. Furthermore, such discharges provide a window for controlling additional discharge parameters viz. enhancement of electron confinement, electron heating, transport of particles, sheath potential, plasma uniformity etc. [5-6]. that can highly impact plasma properties; hence meeting the rapidly rising requirements of semiconductor fabrication industries. The rapid growth of semiconductor industries has led to the requirement of processing larger wafer sizes. Plasma-based processing has also become an important tool used in the semiconductor industry. Hence, the radial uniformity of plasma parameters over large areas is a fundamental challenge that needs to be addressed [7-8]. The present work addresses the strong effect of applied magnetic field on the radial distribution of plasma that can be tailored to improve the plasma uniformity.

This paper is structured in the following manner. In Section 2, we briefly introduce the experimental set-up for producing transverse magnetic field along with the diagnostics used for performing the experiment.

Corresponding author
e mails: sharmanuravi000@gmail.com (*Anuravi Sharma*); *rams@dese.iitd.ac.in* (*Ramesh Narayanan*)

In Section 3, the observed results are discussed in detail. Finally, we conclude by summarizing the important results in Section 4.

2 Experimental Setup

Experiments were performed in a single frequency (13.56 MHz) Capacitively Coupled Discharge (CCD) using argon gas. A detailed schematic of the system is shown in Fig 1. It is a stainless-steel chamber, 30 cm in height and 25 cm in diameter, equipped with parallel electrode geometry. The electrode configuration comprises of two stainless steel (ss) discs with diameter of the upper powered (PE) electrode being 15 cm and lower grounded (GE) electrode being 15.7 cm separated by a distance, $d \approx 7.5$ cm. A 13.56 MHz RF Generator (SEREN R1001) with an automatic matching network (SEREN Model MC2) controller was used to couple RF power from generator to plasma load with maximum efficiency. The vacuum arrangement includes a rotary pump (Oerlikon D160) for low vacuum and a turbo molecular pump (Pfeiffer HiPace80) for generating high vacuum inside ss chamber, with pressure monitored using a set of gauges (Pirani MKS 925, Baratron *MKS 626A*, cold cathode *MKS Series 903*). A cylindrical stainless-steel ground shield is used to cover powered electrode. The lower electrode plate along with the conducting chamber walls are grounded by connecting them to the grounds of RF generator and Matching Network (MN). Experiments were carried out in asymmetric arrangement with the grounded electrode comprising of the entire chamber.

The matching network consists of an inductor and a tuning capacitor connected in a series between RF generator and powered electrode. The PE floats at high voltage, as the capacitance formed by the plasma sheath on one side and the tuning capacitor on the other side provides a DC isolation. Argon gas was utilized to create plasma at filling gas pressures (pfill) ranging from 5 mTorr to 500 mTorr, with a constant RF power input of 10 W.

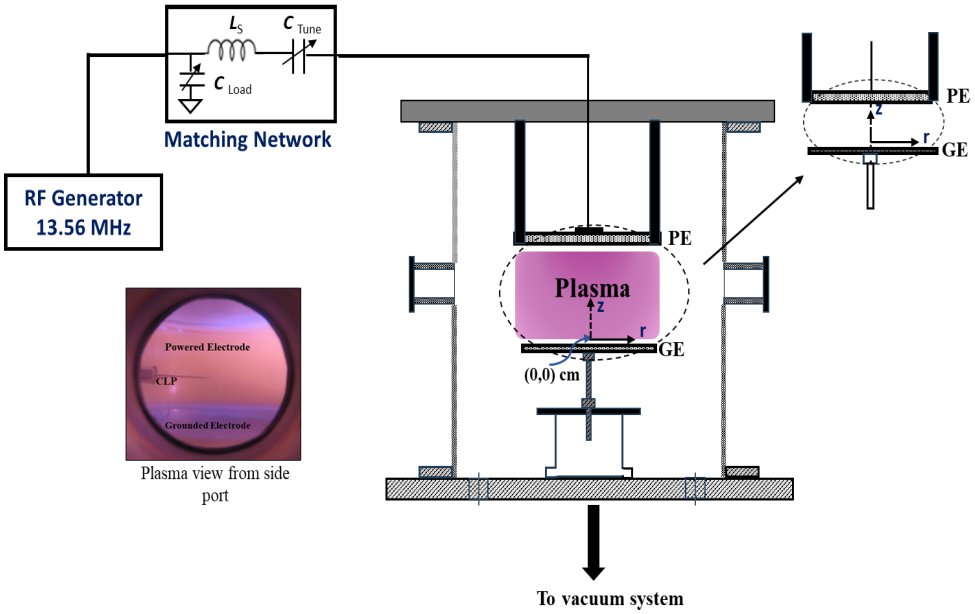

Fig 1. Schematic of experimental setup for Capacitively Coupled Discharge system showing details of electrode configuration and rf circuit.

2.1 Plasma diagnostics used

All the measurements are conducted using RF-compensated Langmuir probes that can be positioned both radially and axially within the plasma environment. The probe utilized in this work incorporates a

tunable three-stage filter circuit at its end, which was designed, fabricated, and calibrated according to the methodology outlined by Ganguli *et al* [9]. The newly developed probe structure (Fig 2(a)) is specifically designed for operation in RF environments, featuring a filter mechanism tuned simultaneously at 13.56 MHz (f), 27.12 MHz (2f) and 40.68 MHz (3f) as shown in Fig 2(b). The calibration procedure of this axial compensated Langmuir probe ensures that the tuned filter box remains unaffected by the presence or absence of plasmas. The response of three stage filter circuit obtained using impedance analyzer is shown in Fig 2(b).

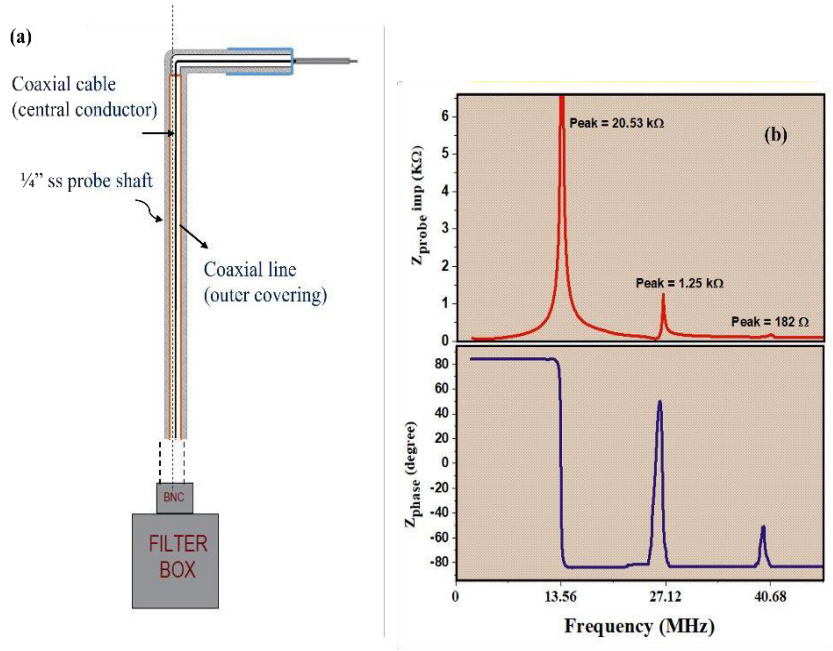

Fig 2. (a) Schematic of axial Compensated Langmuir probe (b) Frequency response of the three-stage filter probe impedance: magnitude (top part) and phase (bottom part).

2.2 Modified setup with magnets

The system is magnetized using two external permanent ring magnets, each having an outer diameter of 152 mm, inner diameter of 116 mm and width of 40 mm, generating a DC magnetic field parallel to the surface of electrodes. [10]. The magnets are configured to produce a homogeneous magnetic field ~ 60G in between the electrodes. The magnetic field strength obtained using COMSOL software (as shown in Figs 3(c) and 3(d)) has also been verified using a Digital Gauss meter (DGM-2024). The cross-sectional and top views of the complete setup with chamber is shown in Fig 3. For the present experiments, distance (d) is kept as 10 cm to produce the required magnetic field strength.

3 Results and Discussions

The experiments presented in this article compares the effect of magnetic field on CCDs with that of the unmagnetized case. All CCD discharges, presented, are operated at 10 W, 13.56 MHz RF power. This set of experiments were performed using axial compensated Langmuir probe mounted from the bottom port of the chamber as shown in Fig 3(a). The radial plasma characteristics are plotted from (r = –6 cm) to (r = 6 cm) at z = 3 cm to analyze plasma profiles from one electrode edge to the other. Despite the axially symmetric nature of the unmagnetized system, the presence of a magnetic field can significantly disturb

this symmetry, as corroborated by the experimental results. The radial plasma density for an unmagnetized discharge is found to have a symmetric profile, with a peak in the center and a fall towards the edges, as previously predicted [11].

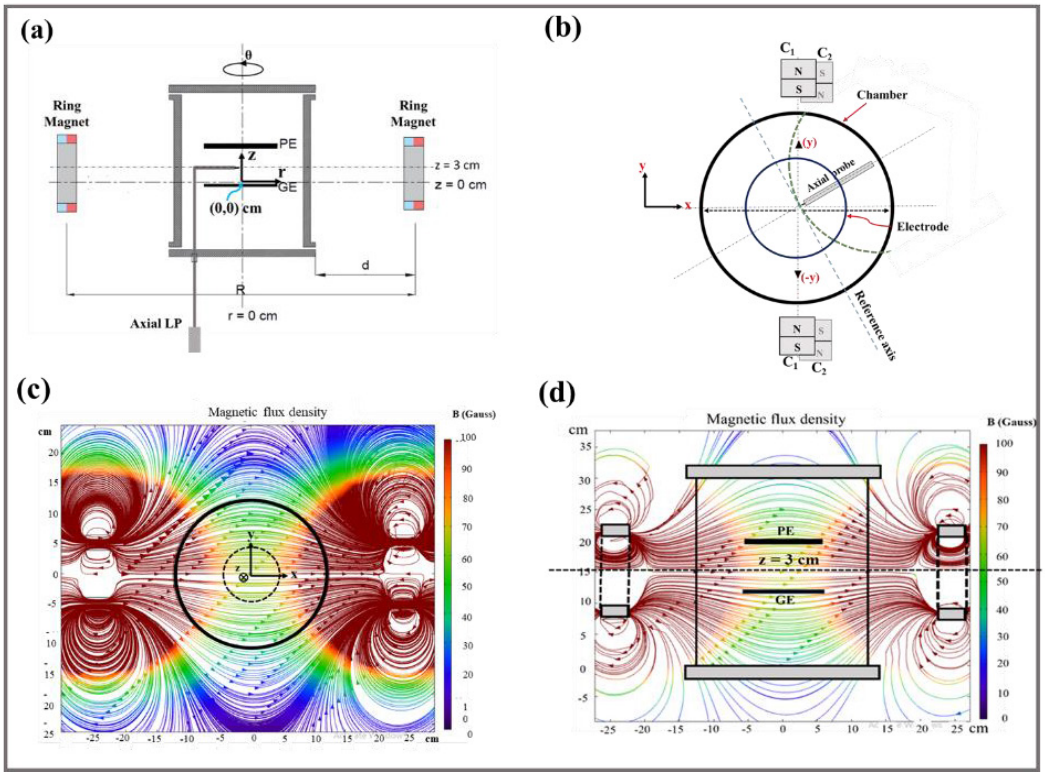

Fig 3. Schematic of the Experimental Set up (a) A cross sectional view of the positioning of two permanent ring magnets with respect to the powered (PE) and grounded (GE) electrodes of the Capacitively Coupled plasma Discharge (CCD) system. The Langmuir probe (LP) is mounted from the bottom port that can be moved along z direction and can be rotated about the axis of the LP shaft in the XY plane. The (x, y, z) coordinate system is chosen such that the origin is at the centre of the circular GE. (r, θ, z) represents the cylindrical coordinate system of the CCD vacuum chamber; (b) The top cut view of the LP measurement plane (XY Plane). The LP measurement is carried out along the dashed arc as shown. C1-C1 represents a typical orientation of the two permanent ring magnets with the line passing through the axis of the two ring magnets subtending an angle θ with respect to probe tip axis passing through the centre of the electrode. C_2-C_2 orientation is just a 180^o rotation of C_1-C_1 about the chamber vertical axis; A typical magnetic field profile plotted in COMSOL software in the (c) XY plane at z = 3 cm; (d) XZ plane at y = 0 cm. It can be clearly seen that the magnetic field lines between the PE and GE remain horizontal, i.e. parallel to the electrode surface.

The results examined the spatial profile variations of plasma under the influence of the magnetic field and its effects across different pressure regimes. In this set of experiments, measurements have been undertaken at four gas filling pressures: 5 mTorr, 40 mTorr, 80 mTorr, and 400 mTorr. Figure 4 shows plots of electron density n_e, electron temperature T_e and plasma potential V_p versus the radial position (r) in different pressure regimes (intermediate (5mTorr, 40 mTorr) & high (80 mTorr, 400 mTorr)) [12] for an unmagnetized plasma [B = 0], shown as black solid line with filled circle symbol. The figure also shows the plasma parameters for two different magnetic field configurations using two permanent ring magnets with its axis parallel to

the plane of the electrode. These two ring magnets are placed diametrically opposite to the experimental chamber as shown in Fig 3(a). The line connecting the axis of the two ring magnets is at an azimuthal angle θ with respect to the reference axis as shown in Fig 3. The experiments were carried out with the magnets placed in two orientations (i) In the first orientation the angle θ is 45° clockwise [C_1-C_1 in Fig 3(b)]; plasma parameters are shown as blue dotted line with rhombus symbol in Fig 4, (ii) Second orientation is realized by azimuthally rotating C_1-C_1 by 180° (C_2-C_2 in Fig 3(b)) with the plasma parameters shown as red dotted line with circle symbol in Fig 4. These three orientations are referred to as B = 0, B(+45°) and B(–45°) in all further references within this paper. Herein, one observes that the magnetic field has significant effect on the plasma parameters at lower pressures as compared to the unmagnetized case. In the presence of the magnetic field, one observed that the plasma density is enhanced along with the electron temperature and plasma potential attaining lower values along the measurement axis. This can be attributed to a better confinement of the gyrating charged particles about the magnetic field [13]. In fact, the influence of applied magnetic field significantly enhances plasma density at a pressure of 5 mTorr, compared to when no magnetic field is present. One, further observes that in the B(+45°) or B(–45°) orientations, the plasma parameters show a shift from the centre-peaked radial profile (for unmagnetized case) to a edge-peaked radial profile (for other two orientations). This observed shift aligns precisely with the direction of the $\vec{E} \times \vec{B}$.

The strongest DC electric field is expected to be in the $\hat{z}$ direction due to the development of the negative self-bias voltage at powered electrode along with applied magnetic field (B) at $\hat{y}$ and $-\hat{y}$ induces $\vec{E} \times \vec{B}$ drift in $-\hat{x}$ and $\hat{x}$ direction, respectively (see Fig 3(b)), even though a majority of this potential difference would be developed across the electrode sheath itself.

3.1 Comparison of plasma parameters with and without magnetic field

The radial profiles are seen to shift from a center-peaked profile for an unmagnetized case to an edge-peaked profile for the magnetized case. At 5 mTorr (Fig 4(a)) the density increases from 1×10^{10} cm^{-3} at the center without any magnetic field to 1.8×0^{10} cm^{-3}. However, the radial profile is observed to not only shift to higher density values but also has changed its profile with a flatter region on either side of the center. For $r < -2$ cm, the densities are constant at 1.5×10^{10} cm^{-3} and for $r > 0$ cm, one finds the densities to be about 1.8×10^{10} cm^{-3}. The region, -2 cm $< r < 0$ cm, tends to be a transition region for the density shift. The reversal of the magnetic field direction from $\theta = 45°$ to $\theta = -45°$ (C_1 to C_2 configuration as shown in Fig 3(b) shows an approximate mirror inversion of the radial profile, as expected. The effect of the magnetic field on the plasma parameters is slightly different at the intermediate pressure regime (40 mTorr). Herein, one does not observe any significant change in the plasma parameters except for the slight shifting of the density peak towards the radial edge. On the other hand, at higher pressure regimes, the magnetic field is found to lower the plasma density. The counter-intuitive effect of the magnetic field-induced plasma density reduction at higher pressures is due to the electron gyrofrequency becoming comparable to the collision frequency at these pressures. For a pressure of 5 mTorr, the presence of a magnetic field results in a decrease in both electron temperature (T_e) and plasma potential (V_p) compared to the unmagnetized state. However, at intermediate and high pressures, these parameters remain nearly similar regardless of the presence of the magnetic field. Within each pressure regime, magnetized plasma exhibits consistent trends for electron temperature, plasma potential, and plasma density profiles. Specifically, for a particular orientation of the magnet, the direction of increase and decrease for all plasma parameters remains the same across different spatial regions. The variation of the plasma parameters across the different pressure regimes due to the presence of the magnetic field shows a significant influence of the latter on CCDs. Figure 5 shows the comparison of the radial profiles of plasma density of the CCDs for the unmagnetized (B = 0) and two magnet orientations B (+45°) and B (–45°). In an unmagnetized CCD discharge, the radial scan of the plasma density displays a symmetric profile, with the lowest density at 5 mTorr and the highest at 400 mTorr.

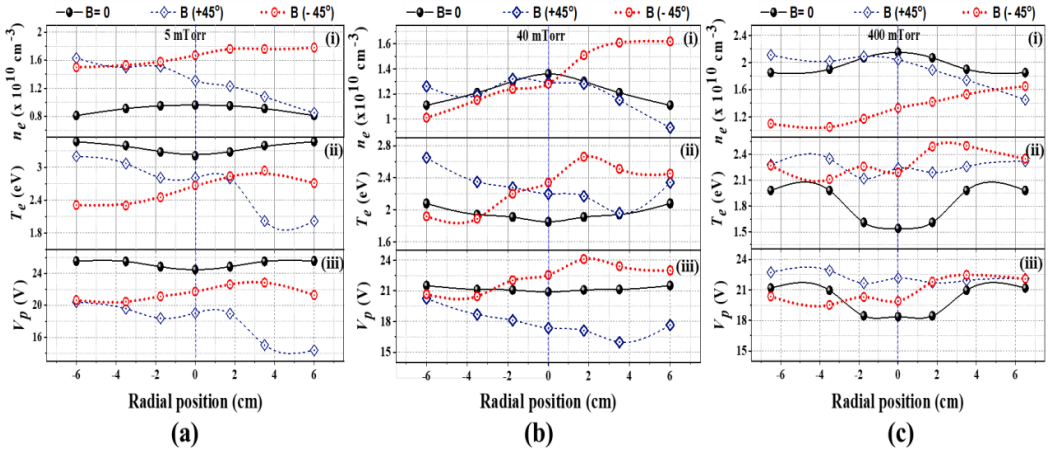

Fig 4. Radial plots of (i) plasma density (n_e), (ii) electron temperature (T_e) & (iii) plasma potential (V_p) for different operating pressures (pfill), viz., (a) 5 mTorr (low pressure regime) (b) 40 mTorr (intermediate pressure regime) (c) 400 mTorr (high pressure regime).

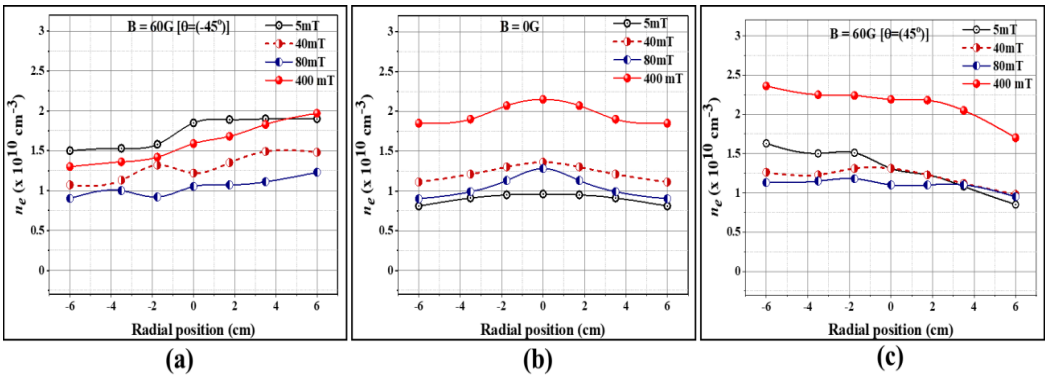

Fig 5. Plasma density radial profiles compared for different pressures in the presence of (a) Magnetic field in C_1 configuration ($\theta = -45^o$), (b) without magnetic field (c) Magnetic field in C_2 configuration ($\theta = 45^o$).

This is primarily due to the increased number of collisions that result in effective ionization with an increase of pressure. The plasma density exhibits distinct patterns across different pressures, both with and without the influence of a magnetic field. The maximum enhancement of plasma density occurs at 5 mTorr for both cases, B at $\theta = 45^o$ & $\theta = -45^o$, because the electron gyrofrequency (ω_{ce}) is significantly higher than the collision frequency (ν_c), where ν_c is the momentum transfer frequency of electrons (at temperature T_e) [3]. The values of some important parameters are mentioned in Table 1. Consequently, electron-neutral collisions do not disrupt the confinement of electrons. At 40 and 80 mTorr, the density noticeably moves from the center to the edge and rises, but at 400 mTorr, both with and without a magnetic field, it stays nearly the same.

3.2 Magnetic field effect on the electron temperatures

The experimental observation shows contradictory variation of electron temperature with and without magnetic field in different pressure regimes. To understand this, one needs to estimate the Hall parameter ($\omega_c\tau_m$) for electrons, where ω_c is the cyclotron frequency and τ_m is inverse of momentum transfer collisional frequency (ν_m). It may be noted that the ions are unmagnetized in these set of experiments since, even at the lowest pressure (5 mTorr), the ion-neutral collision mean free-path ($\lambda_i \sim 6$mm) is much smaller

than the ion Larmor radius (r_{Li} ~ 24mm). Figure 6 shows a plot of ($\omega_c\tau_m$) and the perpendicular mobility term (μ_m) as a function of pressure. It clearly shows the dominance of ($\omega_c\tau_m$) term at low pressures, while at high pressures (above 100 mTorr) it is becoming almost negligible.

Table 1. Calculated values of (a) collision frequency at different pressures (b) electron cyclotron frequency at different B values

B (Gauss)	Electron cyclotron frequency ($\omega_{ce}\times10^8$sec^{-1})	Pressure (m Torr)	Collision frequency ($\nu_c\times10^8$sec^{-1})
2.42	0.42	100	3.5
5	0.875	80	2.8
10	1.75	60	2.1
20	3.5	40	1.4
25	4.37	35	1.2
30	5.25	20	0.7
40	7	15	0.52
50	8.75	10	0.35
60	10.5	5	0.17
65	11.3	1	0.035

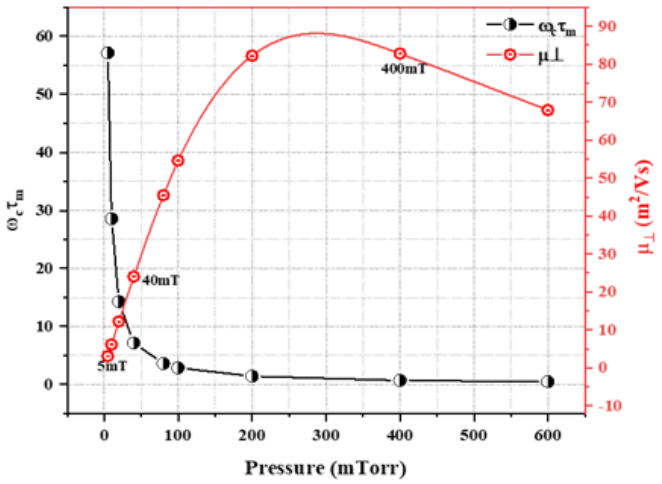

Fig 6. Plots of hall parameter ($\omega_c\tau_m$) and $\mu_\perp$ with varying pressure.

The perpendicular diffusion ($D_\perp$) and perpendicular mobility term ($\mu_\perp$) are given as [3],

$$D_\perp = \frac{D}{1+(\omega_c\,\tau_m)^2} \tag{1a}$$

$$\mu_\perp = \frac{\mu}{1+(\omega_c\,\tau_m)^2} \tag{1b}$$

Hence, $D_\perp$ and $\mu_\perp$ are least for low pressures and increases for higher pressures [3]. A typical variation of $\mu_\perp$ with pressure is also given in Fig 6. The plots for parallel and perpendicular diffusion coefficients are compared in the presence and absence of magnetic field as shown in Fig 7. These plots clearly demonstrate that $D_\parallel$ decreases at lower pressures and increases at higher pressures in the presence of magnetic field.

Additionally, $D_\perp$ increases significantly with rising pressure, potentially leading to greater electron loss and, consequently, an increase in electron temperature to sustain the plasma.

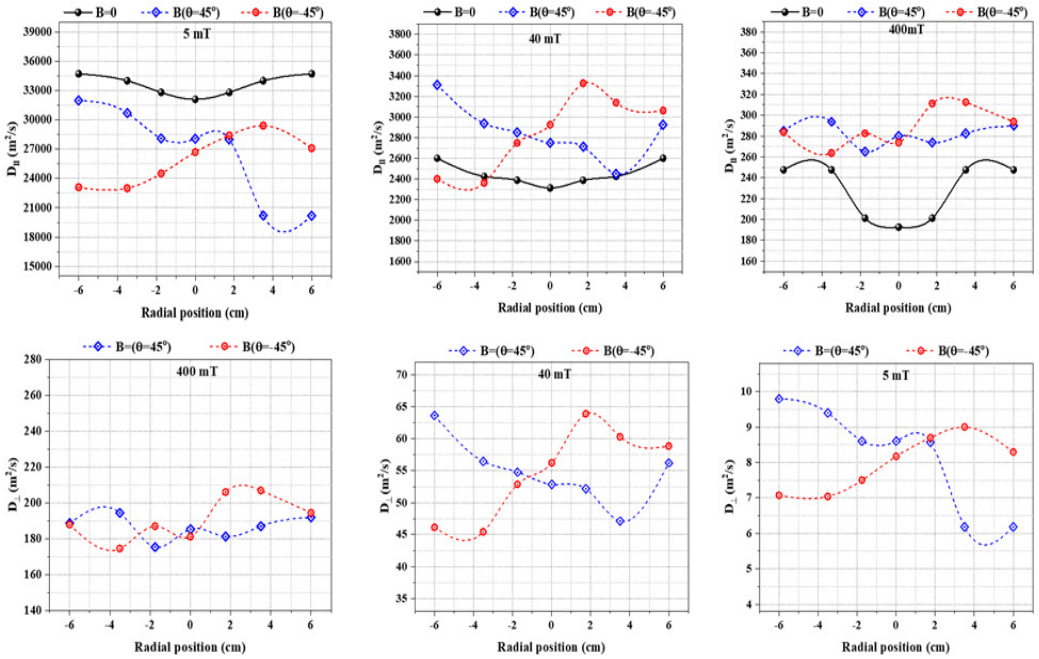

Fig 7. Plots of $D_{||}$ and $D_\perp$ at (a) 5mTorr (b) 40mTorr (c) 400mTorr.

For understanding this behavior, one estimates the total perpendicular drift experienced by electrons in vector form from the relation [3].

$$\vec{u}_\perp = \pm \mu_\perp \vec{E} - D_\perp \frac{\vec{\nabla} n}{n} + \frac{(\vec{u}_E + \vec{u}_D)}{1 + (\omega_c \tau_m)^{-2}} \tag{2}$$

Expanding the $\vec{E} \times \vec{B}$ drift term ($\vec{u}_E$) and the diamagnetic drift term ($\vec{u}_D$), one gets,

$$\vec{u}_\perp = \pm \mu_\perp \vec{E} - D_\perp \frac{\vec{\nabla} n}{n} + \frac{1}{B^2(1 + (\omega_c \tau_m)^{-2})} (\vec{E} \times \vec{B}) - \frac{T_e(eV)}{B^2(1 + (\omega_c \tau_m)^{-2})} \left(\frac{\vec{\nabla}_n \times \vec{B}}{n} \right) \tag{3}$$

In this set of experiments the magnetic field $(\vec{B})$ is directed along the $\hat{y}$ direction whereas the electric field $(\vec{E})$ is along the $(\hat{x}, \hat{z})$ direction. The dc electric fields, considered for this model, is that present within the plasma due to the negative gradient of the plasma potential (V_p). It may be noted that this field is relatively weak in comparison to the voltage drops across the electrode sheaths. This is being considered since the plane of measurement is away from the region of these strong electrode sheaths. Hence, if one resolves Eq (3) into its different components, primarily in the x - y plane. i.e. parallel to the substrate plane, one has:

$$u_y = \pm \mu_{||} E_y - D_{||} \left(\frac{1}{n(y)} \frac{dn}{dy} \right) \tag{4a}$$

$$u_x = \pm \mu_{\perp,x} E_x - D_{\perp,y} \left(\frac{1}{n(x)} \frac{dn}{dx} \right) + \frac{1}{1 + (\omega_c \tau_m)^{-2}} \left(\frac{E_z}{B} \right) - \frac{T_e(eV)}{B(1 + (\omega_c \tau_m)^{-2})} \left(\frac{1}{n(z)} \frac{dn}{dz} \right) \tag{4b}$$

$$u_z = \pm \mu_{\perp,z} E_z - D_{\perp,x}\left(\frac{1}{n(z)}\frac{dn}{dz}\right) + \frac{1}{1+(\omega_c\tau_m)^{-2}}\left(\frac{E_x}{B}\right) - \frac{T_e(eV)}{B(1+(\omega_c\tau_m)^{-2})}\left(\frac{1}{n(x)}\frac{dn}{dx}\right) \quad (4c)$$

The contributions of the different terms on the right hand side of the three equations in Eq (4) are calculated for three different pressures (5 mTorr, 40 mTorr and 400 mTorr). These estimated values are given in Tables 2 and 3. Other parameters (ω_c, τ_m, T_e) were evaluated using the plasma parameters estimated from the LP measurements. It is to be noted that, in this work, one is primarily interested in the drifts occurring in the x-y plane (i. e. parallel to the electrode planes). Hence, the axial electric field (E_z) is an important parameter to be considered. Based on the plasma parameters measured in these set of experiments, one has estimated that the axial electric field (E_z), ranging from 25-100 V/m is the most dominant electric field in the pressure regimes considered in this article. Thus one sees that E_z = 80 V/m for 5 mTorr and E_z = 20 V/m for 40 mTorr and 400 mTorr whereas the inverse axial density scale length term $\left.\frac{\nabla n}{n}\right|_z = \frac{1}{n(z)}\frac{dn}{dz}$ is estimated to be about ~ 10 m^{-1}, i. e. for maximum density gradient along axis [19]. The voltage drop across x and y is very small (~2V), across the radial extent of the electrode (radius = 7.5 cm). Hence, one can approximate E_x and E_y to be 25V/m for all pressures with the maximum density scale length term $\left.\frac{\nabla n}{n}\right|_{x,\,y}$ is estimated to be ~ 10 m^{-1} along x-y plane.

Table 2. Calculated values of different terms present in Eq (4)

Pressure term (m Torr)	Mobility term $(\mu_{\parallel} E_y)$ (m/s)	Diffusion term $\left[D_{\parallel}\left(\frac{1}{n(z)}\frac{dn}{dz}\right)\right]$ (m/s)	Mobility term $(\mu_{\perp x} E_x)$ (m/s)	Mobility term $(\mu_{\perp x} E_z)$ (m/s)	Diffusion term $\left[D_{\perp,z}\left(\frac{1}{n(z)}\frac{dn}{dz}\right)\right]$ (m/s)	Diffusion term $\left[D_{\perp,z}\left(\frac{1}{n(x)}\frac{dn}{dx}\right)\right]$ (m/s)
5	250000	2.6×10^5	76.5	244.8	86	86
40	31250	2.7×10^4	600.75	540.6	528.6	528.6
400	3125	2.8×10^3	2069.25	1655.4	1854.1	1854.1

Table 3. Calculated values of different terms present in Eq (4)

Pressure mTorr	$\vec{E}\times\vec{B}$ drift term $\frac{1}{(1+(\omega_c\tau_m)^{-2})}\frac{E_z}{B}$ m/s	$\vec{E}\times\vec{B}$ drift term $\frac{1}{(1+(\omega_c\tau_m)^{-2})}\frac{E_x}{B}$ m/s	Diamagnetic drift term $\frac{T(\text{eV})}{B(1+(\omega_c\tau_m)^{-2})}\left(\frac{1}{n(z)}\frac{dn}{dz}\right)$ m/s	Diamagnetic drift term $\frac{T(\text{eV})}{B(1+(\omega_c\tau_m)^{-2})}\left(\frac{1}{n(x)}\frac{dn}{dx}\right)$ m/s
5	13328	4166.6	3998.7753	3998.7753
40	3269.2	4084.9	3923.0467	3923.0467
400	1125.4	1406.9	1350.6355	1350.6355

From Table1, one can see that at low pressures (5 mTorr) $\vec{E}\times\vec{B}$ drift is more dominant, while at high pressures, the first two terms ($\mu_{\perp}$ and $D_{\perp}$) are more prominent. Thus, at lower pressures, the applied magnetic field has been observed to be highly effective resulting in more confinement of electrons while at high pressures the effect of magnetic field is almost negligible and there could be increased losses due to high values of $\mu_{\perp}$ and $D_{\perp}$ that eventually leads to a decrease in plasma density. This decrease in plasma density is attributed to an enhanced loss of charged particles (primarily electrons due to its high mobility)

from the bulk of the plasma. The plasma will then tend to self-organize itself to maintain its quasi-neutrality. This is self-consistently triggered by the plasma raising its plasma potential so as to mitigate the bleeding of the electrons from the bulk region towards the boundaries (electrodes or chamber wall) and simultaneously allowing for ions to be accelerated towards the chamber walls.

Simultaneously, an increase of electron temperatures, at higher pressures, indicates the possibility of higher ionization rates to supplement the losses from the plasma bulk. It may be noted that, for the temperatures of interest in this work, one can correlate temperature increase with enhanced ionization rates [3]. Thus one can summarize, that the observation of decrease of electron temperature and increase of plasma density at lower pressures to be associated with an enhanced confinement of plasma while, on the other hand, the increased losses at higher pressures could be identified as the reason for increased temperature and reduced density in the presence of magnetic fields.

3.3 Effect of Rotating Magnets on plasma parameters

To further verify the effect of $\vec{E} \times \vec{B}$ drift on plasma, magnets, oriented in the C_1 - C_1 and C_2 - C_2 configurations of Fig 3(b), is rotated such that, the angle θ is changed to different angles with respect to measurement axis. For the experiments presented in this study, θ was kept at 60°, 90° and 120° (Fig 8). This experimental approach allows for a comprehensive understanding of how, ($\vec{E} \times \vec{B}$) drift and related phenomena influence plasma behavior in the azimuthal direction [14,15]. A radial compensated Langmuir probe, inserted through a side port of the cylindrical chamber is employed in these experiments.

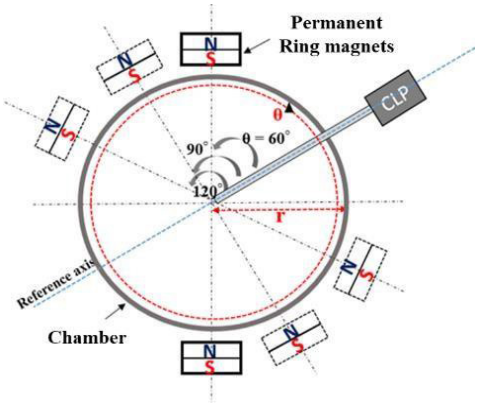

Fig 8. Top view of the experimental setup showing profile plasma magnets placed at different orientations.

The radial density is plotted from (r = –7.5 cm) to (r = 7.5 cm) at z = 3.75 cm. Figure 9 shows radial plots of plasma density (blue dotted line, open rhombus symbol) for three different orientations of the C_1-C_1 magnet configuration (i.e. $\theta = 60^o$, 90^o, 120^o as shown in Fig 8). A similar set of radial profiles are plotted in Fig 9 (red, dotted line, open circle symbol), for three different orientations of the C_2 - C_2 magnet configuration (not shown in Fig 8). The plasma parameters in these orientations are compared with that of the unmagnetized CCD configuration (black solid line, filled circle symbol). These plasma density plots are for measurements in the intermediate (40 mTorr in Fig 9(a)) and high (200 mTorr in Fig 9(b)) pressure regimes. As mentioned previously, the effect of magnetic field for each orientation is different in both pressure regimes. The plasma density profile, if compared for each orientation of magnets (θ = 60°, 90°,120°) with that of the unmagnetized case is found to be remaining almost similar at the center but increasing towards the edges in the presence of magnetic fields. This can be attributed to drifts associated with these magnetic fields [16]. The maximum enhancement is at θ = 90°, since the effect of $\vec{E} \times \vec{B}$ is maximum in the direction perpendicular to the Electric field ($\vec{E}$) and Magnetic field ($\vec{B}$). Figure 9(b) depicts a contrasting influence

of magnetic field on the plasma parameters. On the other hand, one observes a contrasting feature at high pressures (200 mTorr) in Fig 9(b) wherein the plasma density has decreased at the center, while remaining almost same at the edges, for each orientation. The above results indicate a strong correlation between ω_{ce} (term proportional to magnetic field) and ν_c (term that is a function of pressure, with $\nu_c = 1/\tau_m$) in the transport of particles across different pressure regimes for a given magnetic field strength (B). This effect can be clearly visible if one looks at Eq (4), wherein the term $\omega_c\tau_m$ (= ω_c/ν_c) determines the dominance of some of the terms on the right-hand-side of the three equations. Hence, it is expected that the control of the plasma dynamics using external magnetic fields across different pressure regimes will depend on the choice of the appropriate magnetic field strength for a given pressure regime.

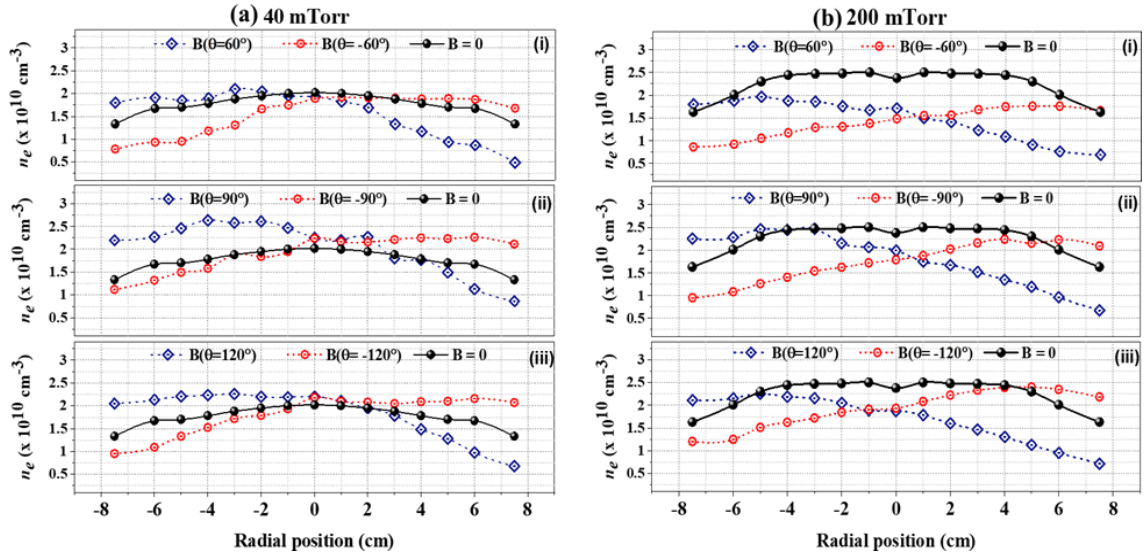

Fig 9. Radial profiles of plasma density without magnetic field (B = 0) compared with profiles in the presence of magnetic field for B at (θ = (i) 60°, (ii) 90° & (iii) 120°) for two different gas filling pressures (p_{fill}) (a) 40 mTorr (b) 200 m.

4 Summary

To summarize, the article presents a comparison of the radial profiles of the plasma parameters of an unmagnetized capacitively coupled discharge (CCD) with that of a magnetized CCD. The experimental approach for configuring the latter is to have a pair of permanent ring magnets to generate a horizontal magnetic field that is parallel to the electrode surface. The direction of this horizontal field is changed by rotating the line joining the two ring magnets along the azimuthal plane; the reference point being the axis of the Langmuir probe used to measure the radial profiles. This variation of the orientation enables one to identify the azimuthal variation of the plasma parameters for a given horizontal magnetic field strength. These set of experiments have been carried out for various pressures. The experimental observations have identified that the ratio of the cyclotron frequency (ω_c) to that of the collision frequency (ν_c) is a determining factor to identify if the given capacitively-coupled discharge would be magnetically-coupled. The horizontal magnetic field is seen to trigger a $\vec{E}\times\vec{B}$ drift. This drift results in the shifting of the peak in the radial plasma density profile towards the edge. Further, it is also noted that for the set of parameters, shown in this article, the magnetic field is seen to have a stronger effect on plasma confinement in the bulk region at lower pressures whereas at higher pressures the magnetic field strengths are not significant to be dominant then the diffusive and drift losses.

In conclusion, one can infer that even though the current magnetic field configuration tends to introduce an asymmetry in the plasma profile, the fact that the plasma density can be enhanced at lower pressures is indicative that a suitable magnetic field configuration would enable a more uniform radial plasma profile for a magnetized CCD. For this purpose, the direction of $\vec{E}\times\vec{B}$ drift could be adjusted suitably by modifying the magnetic field configuration to achieve the desired outcomes. Studies with other magnetic field configurations are underway and will be reported in future work. These results have implications in the plasma processing industry where large area, batch processing can be accomplished more economically.

Acknowledgment

The authors would like to thank Prof A Ganguli (Retired faculty, IIT Delhi) and Dr A Rawat (Impedans Ltd, Dublin) for valuable inputs related to the above work. They also acknowledge Central Research Facility (CRF), IIT Delhi for providing utility of CRF facilities for various fabrication work required during the experiments. The experimental system was partially supported by Department of Atomic Energy, India (BRNS) [BRNS Ref: 2012/34/4/BRNS/125, IITD ref: RP02601] and the above work was also partially supported from Core Research Grant (CRG), Science & Engineering Research Board (SERB), DST [SERB Ref: CRG/2021/004273, IITD ref: RP04275G].

References

1. Donnelly V M, Kornblit A, Plasma etching: Yesterday, today, and tomorrow, *J Vac Sci Technol*, A 31(2013)050825; doi.org/10.1116/1.4819316.
2. Paranjpe A P, Moslehi M M, Davis C J, Modelling the uniformity in a magnetron etching system, *J Vac Sci Technol*, A 10(1992)1140–1146.
3. Lieberman M A, Lichtenberg A J, Principles of Plasma Discharges and Materials Processing, (New Jersey: Wiley), 2005.
4. Chabert P, Braithwaite N, Physics of Radio-Frequency Plasmas, (New York: Cambridge University Press), 2011.
5. Wilczek S, Trieschmann J, Schulze J et al., The effect of driving frequency on the confinement of beam electrons and plasma density in low-pressure capacitive discharges, *Plasma Sources Sci Technol*, 24(2015)024002; doi. 10.1088/0963-0252/24/2/024002.
6. Oberberg M, Kallähn J, Awakowicz P, Schulze J, Experimental investigations of the magnetic asymmetry effect in capacitively coupled radio frequency plasmas, *Plasma Sources Sci Technol*, 27(2018)105018; doi. 10.1088/1361-6595/aae199.
7. Liu Y, Booth J P, Chabert P, Effect of frequency on the uniformity of symmetrical RF CCP discharges, *Plasma Sources Sci Technol*, 27(2018)055012; doi. 10.1088/1361-6595/aabfb4.
8. Das S, Karkari S K, Radial control of plasma uniformity and electron temperature by external plate biasing in a back diffused partially magnetized plasma, *Plasma Res Express*, 3(2021)025013; doi. 10.1088/2516-1067/ac0a43
9. Ganguli A, Sahu B B, Tarey R D, A new structure for RF-compensated Langmuir probes with external filters tunable in the absence of plasma, *Plasma Sources Sci Technol*, 17(2008)015003; doi. 10.1088/0963-0252/17/1/015003.
10. You S J, Chung C W, Bai K H, Chang H Y, Power dissipation mode transition by a magnetic field, *Appl Phys Lett*, 81(2002)2529–2531.
11. Joshi J K, Karkari S K, Kumar S, Effect of Magnetization on Impedance Characteristics of a Capacitive Discharge Using Push-Pull Driven Cylindrical Electrodes, *IEEE Trans Plasma Sci*, 47(2019)5291–5298.
12. Rawat A, Ganguli A, Narayanan R, Tarey R D, Correlation of stochastic and ohmic power absorption with observed RF harmonics and plasma parameters in capacitively coupled discharges, *Plasma Res Express*, 2(2020)035015; doi.10.1088/2516-1067/abb56f.
13. Tsankov T V, Chabert P, Czarnetzki U, Foundations of magnetized radio-frequency discharges, *Plasma Sources Sci Technol*, 31(2022)084007; doi. 10.1088/1361-6595/ac869a.

14. Zhou J, Liao J, Huang J, Chen T, Lv B, Peng Y, Effects of process parameters and chamber structure on plasma uniformity in a large-area capacitively coupled discharge, *Vacuum*, 195(2022)110678; doi.org/10.1016/j.vacuum.2021.110678
15. Wickramanayaka S, Nakagawa Y, Sago Y, Numasawa Y, Optimization of plasma density and radial uniformity of a point-cusp magnetic field applied capacitive plasma, *J Vac Sci Technol*, A 18(2000)823–829.
16. You S J, Hai T T, Park M, Kim D W, Kim J H, Seong D J, Shin Y H, Lee S H, Park G Y, Lee J K, Chang H Y, Role of transverse magnetic field in the capacitive discharge, *Thin Solid Films*, 519(2011)6981–6989.
17. Menati M, Rasoolian B, Thomas E, Konopka U, Experimental observation and numerical investigation of filamentary structures in magnetized plasmas, *Phys Plasmas*, 27(2020)022101; doi.org/10.1063/1.5135761.
18. Turner M M, Pressure Heating of Electrons in Capacitively Coupled rf Discharges, *Phys Rev Lett*, 75(1995) 1312–1315.
19. Rawat A, Development of diagnostics for characterizing electron heating mechanisms in low pressure RF discharges, Doctoral thesis from Department of Energy Science and Engineering, Indian Institute of Technology Delhi, (2021).

[*Received*: 31.12.2024; *revisd recd*: 19.02.2025; *accepted*: 20.02.2025]